# Mechanism on Traveling-Wave Transport of Particles

*Hiroyuki Kawamoto and Kyogo Seki*
*Department of Mechanical Engineering, Waseda University*
*Shinjuku, Tokyo, Japan*

## Abstract

Numerical and experimental investigations were carried out on transport of particles in an electrostatic traveling field. A 3D hard-sphere model of the Distinct Element Method was developed to simulate dynamics of particles. Forces applied to particles in the model were the Coulomb force, the electrostatic force to polarized particles in the non-uniform field, the gravity, and the air drag. Friction and repulsion between particle-particle and particle-conveyer were included in the model to replace initial conditions after mechanical contacts. Two kinds of experiments were performed to confirm the model. One was the measurement of charge of particles that is indispensable to determine the Coulomb force. Charge distribution was measured from locus of free-fallen particles in a parallel electrostatic field. Averaged charges of bulk particles were confirmed by the measurement with a Faraday cage. The other experiment was measurements of differential dynamics of particles on a conveyer consisting of parallel electrodes to which four-phase traveling electrostatic wave was applied. The calculated results agreed with measured and the following were clarified: (1) Coulomb force is most predominant to drive particles. (2) The direction of particle transport did not always coincide with that of the traveling wave but partially changed depending on the frequency of the traveling wave, the particle diameter, and the electric field. (3) Although some particles overtook the traveling wave at the very low frequency, the motion of particles was almost synchronized with the wave at the low frequency. (4) The transport of some particles delayed to the wave at medium frequency and almost all particles were transported backward at high frequency.

## Introduction

Electrostatic traveling-wave transport of particles has been investigated and fundamental performances have been clarified by a parametric experiment, because it has a potential to realize a sophisticated particle supplier in electrophotography.[1] The technology will be applied not only for an electrophotography developer[2-4] but also for electronic, chemical, and biochemical applications,[5] because it has the advantage that the transport can be controlled through electrical parameters instead of mechanical means and therefore it is free against contamination and the mechanical vibration.

However, although many investigations have been conducted, mechanism of the transport is not clear so far.[6] The reason why former models could not clarify the mechanism thoroughly is that although the motion of particles is affected by many parameters which include interaction between particles and it is not simple and identical but a complex of many modes, they have over-simplified the phenomena.

In this study, a three-dimensional hard-sphere model of the Distinct Element Method was developed to simulate dynamics of particles in the electrostatic traveling field. Charge of particles, which is essentially important to calculate the dynamics, were measured by a free-fallen method in a parallel electrostatic field and a Faraday cage. Microscopic differential dynamics of particles were also observed to confirm the model.

## Experimental

A conveyer and a power supply used for experiments are shown in Fig. 1.[1] The conveyer consists of parallel copper electrodes, 0.5 mm width and 1.0 mm pitch, etched by photolithography on a plastic substrate, 120 mm width and 250 mm length, as shown in Fig. 2. The surface of the conveyer is covered with an insulating film made of acetate rayon (3M, 810-18D) to prevent from electrical breakdown between electrodes.

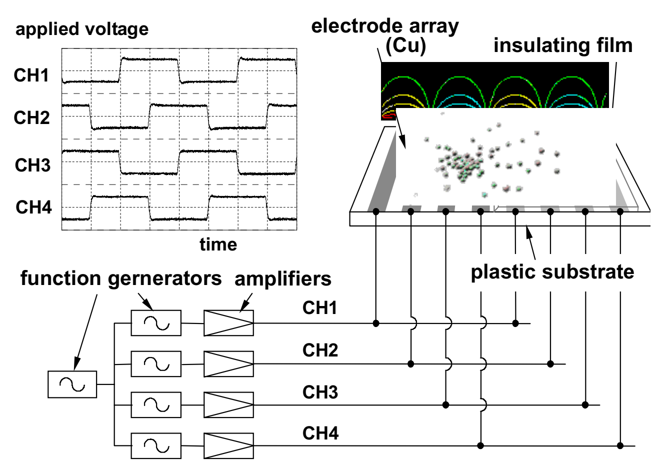


*Figure 1. Particle conveyer and power supply.*

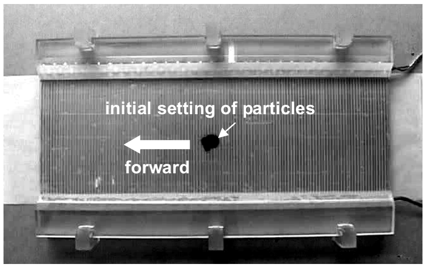


*Figure 2. Photograph of particle conveyer.*

**Table 1. Specification of Particles**

| | ACM 235 | ACM 255 | ACM 288 | ACM 2107 |
|---|---|---|---|---|
| averaged diameter, μm | 29.7 | 47.4 | 72.6 | 106.3 |
| standard deviation, μm | 5.3 | 11.8 | 23.3 | 13.1 |
| density, $kg/m^3$ | 3.50 | 3.52 | 3.62 | 3.50 |
| resistivity, Ωcm | $1\times10^9$ | $2\times10^7$ | $3\times10^9$ | $8\times10^7$ |

Traveling-wave propagation is achieved utilizing four amplifiers (Matsusada Precision, HOPS-1B3) and five function generators (Iwatsu, SG-4105), one of which is used to control phase-differences of the other four generators.1 Rectangular voltage of 800 V, which is a limit against an insulation breakdown of the conveyer, was applied to electrodes.

Four kinds of spherical carrier particles made by the polymerization method (Toda Kogyo) were used for experiments.[1] Specifications of particles are listed in Table 1 and photographs and distributions of particle diameters are shown in Fig. 3. Distribution of particle diameters was derived by an optical method of randomly selected each 3,000 particles.

Microscopic motion of particles was observed to confirm the numerical model with a high-speed microscope camera (Japan Roper, Motion-Meter 1140-0003).

## Charge of Particles

Because charge of particles is essentially important to calculate the dynamics, charging mechanism during transport and the resultant bulk charge were measured by the following two methods.

### Measurement with Faraday Cage

Averaged charge of bulk particles was measured with our in-house-made Faraday cage. It consisted of an inner aluminum pipe of ϕ 25 mm inner diameter, an outer aluminum pipe that is insulated to the inner pipe, and a filter settled in the inner pipe. Particles were vacuum-trapped to the filter and voltage between the inner and outer pipes was measured by an electrometer (Advantest, R8252) to derive total charge of trapped particles. Total weight of particles was measured by an electronic balance (Mettler, SAG105) and an averaged specific charge was deduced.

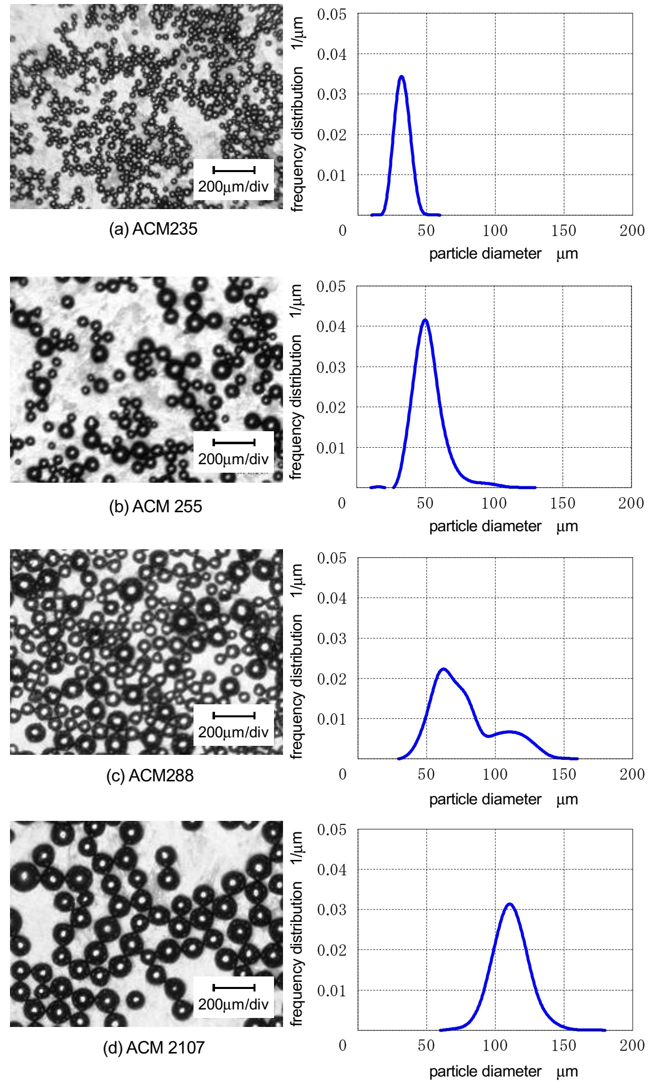


*Figure 3. Photograph of particles and distributions of particle diameter.*

Figure 4 shows the measured specific charge of particles, which were discharged before experiment, with respect to time after 1,000 Hz voltage was applied to the conveyer. At this high frequency particles were not transported in either direction but only vibrated on the conveyer as reported in the reference (1). The following characteristics were deduced from the result. (1) Particles were charged about −0.01 to −0.03 μC/g due to the static contact, at $t = 0$ in Fig. 4, with the insulation film of the conveyer. It was confirmed by the numerical calculation described in the next chapter that this value was large enough to drive particles by the Coulomb force just after the traveling field was applied. (2) Charge of particles was increased in accordance with the increase of the vibration time due to the contact and friction to the film and then converged to a saturated value. This characteristic is common with that of toner particles in the developer of electrophotography.

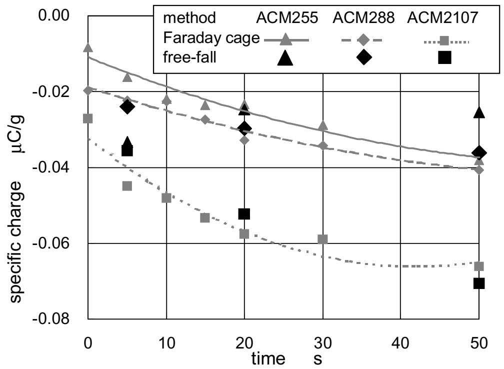


*Figure 4. Charging of particles in contact with insulating film on conveyer.*

## Measurement with Free-Fallen Method

The charge distribution of particles was measured with a free-fallen method in a parallel electrostatic field,[7] because it is indispensable to perform a realistic simulation on the particle transport. Photographs of an apparatus are shown in Fig. 5. Particles transported to the end of the conveyer were free-fallen and introduced in a center between parallel electrodes through a slit. If mechanical and electrostatic interactions between particles were neglected, a particle trajectory ($x$, $y$) was determined by the Coulomb force, the air drag, and the gravity as schematically shown in Fig. 6 (a).

$$m\ddot{x} + 6\pi\eta R\dot{x} = qE(y), \quad m\ddot{y} + 6\pi\eta R\dot{y} = mg \;, \tag{1}$$

where $m$ is a mass of the particle, $\eta$ is the viscosity of air, $R$ is a radius of the particle, $q$ is the charge of the particle, $E$ is the electrostatic field, and $g$ is the gravitational constant. The distribution of the electrostatic field determined by the Laplace equation was calculated by the Finite Element Method and it is shown in Fig. 6 (b). Equation (1) was numerically calculated with the Runge-Kutta method and the charge distribution was implicitly determined from a distribution of trapped particles on an adhesive tape settled at the bottom of the parallel electrodes. A photograph of trapped particles was shown in Fig. 7. Image processing such as the segmentation was applied to the photograph to derive the charge distribution.

Measured charge distributions are shown in Figs 8-10. Parameters were the diameter of particle and the vibration time. In case of '0 s,' particles were directly introduced in the slit without contact with the insulation film but in other cases particles were settled on the conveyer and vibrated with 1,000 Hz wave for the designated time and then introduced in the slit. First of all, it was confirmed that the charge without contact to the insulation film (0 s) was measured to be almost 0 µC/g. This confirmed the adequacy of the experiment. The following two interesting characteristics were deduced from the result. (1) Particles were charged negatively in accordance with the vibration time. Averaged values of the specific charge were deduced from these figures and added in Fig. 4. It is clearly found that the averaged specific charge measured with the free-fallen method agreed well with that of the Faraday cage method. (2) Charge distribution showed two peaks and these separated each other in accordance with time, probably because the polarization between particles took place due to the particle-particle contact.

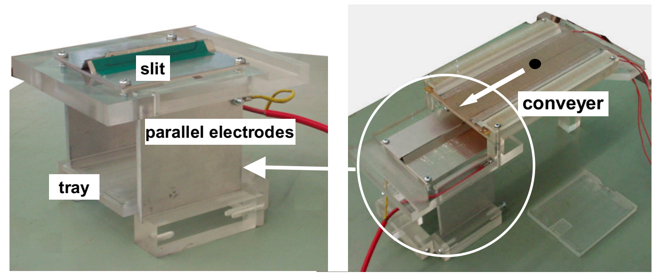


*Figure 5. Photographs of apparatus to measure charge distribution of transported particles.*

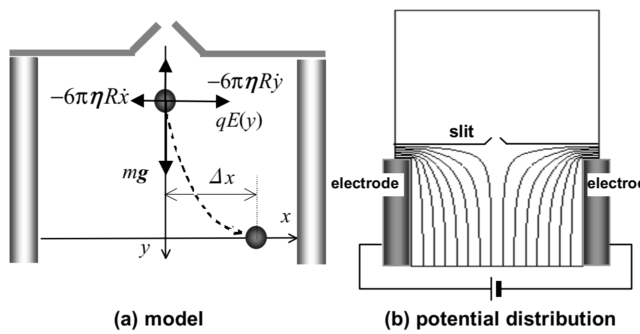


*Figure 6. (a) Forces and trajectory of particle in electric field and (b) potential distribution between parallel electrodes.*

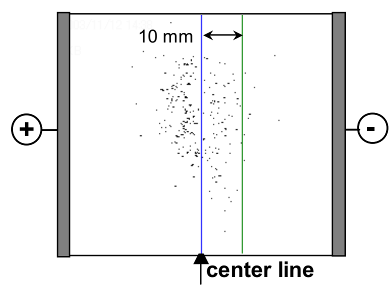


*Figure 7. Trapped particles on tray settled at bottom of parallel electrodes.*

Summarizing these experimental results, we can assume the mechanism of particle charge during the traveling-wave transport.[8] That is, initially discharged particles are charged about −0.01 to −0.03 µC/g when they are settled on the conveyer. This is the static electrification due to the static contact with the insulation film of the conveyer. If the traveling field is applied, the substantial Coulomb force that is enough to drive particles is applied to statically charged particles. Then particles are driven and collide with the film. This increases charge in negative with time but converges to a saturated value. Collision between particles also takes place and this causes the polarization between particles and the distribution of the specific charge separates in two peaks.

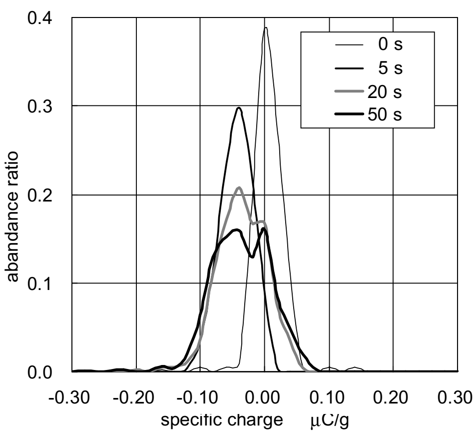


*Figure 8. Charge distributions before (0 s) and after in contact with insulating film on conveyer. (ACM235)*

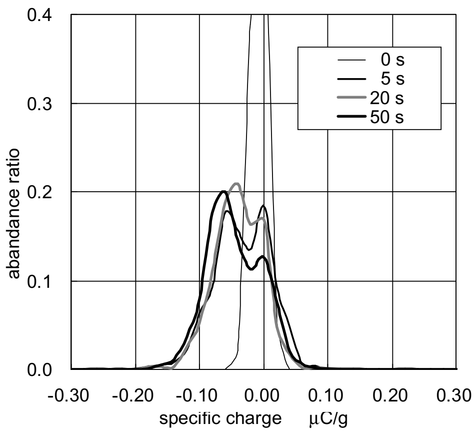


*Figure 9. Charge distributions before (0 s) and after in contact with insulating film on conveyer. (ACM255)*

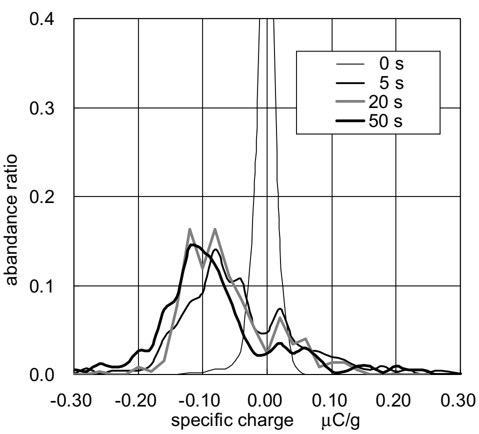


*Figure 10. Charge distributions before (0 s) and after in contact with insulating film on conveyer. (ACM2107)*

## Numerical Simulation

A numerical simulation was conducted based on a three-dimensional hard-sphere mode to clarify the dynamics of the traveling-wave transport of particles. The basic motion equation is a 6-degree-of-freedom system of particle *i*.

$$m_i\ddot{\boldsymbol{x}}_i + 6\pi\eta R\dot{\boldsymbol{x}}_i = q_i\boldsymbol{E} + \boldsymbol{F}_{dipole} + m_i\boldsymbol{g}, \quad I_i\ddot{\boldsymbol{\theta}}_i = 0\ , \tag{2}$$

where $\boldsymbol{x} = (x, y, z)$, $\boldsymbol{\theta} = (\theta_x, \theta_y, \theta_z)$ and $I$ is an inertia of the particle. The electric field $\boldsymbol{E}$ in the term of the Coulomb force consists of the traveling field $\boldsymbol{E}_0$ generated by the power supplies and the electrostatic field $\boldsymbol{E}_q$ created by other charged particles.

$$\boldsymbol{E} = \boldsymbol{E}_0 + \boldsymbol{E}_q = -\nabla\phi + \frac{1}{4\pi\varepsilon_0}\sum_{n\neq i}^{N} q_n \frac{\boldsymbol{r}}{|\boldsymbol{r}|^3}\ , \tag{3}$$

where $\varepsilon_0$ is the permittivity of free space, $\phi$ is the electric potential, $N$ is a number of particles, and $\boldsymbol{r} = (x_i - x_n, y_i - y_n, z_i - z_n)$. The potential distribution $\phi$ is calculated with the two-dimensional Finite Element Method in a cyclic domain of two-pitch width. Parabolic elements were employed for the FEM calculation, because a second order differential is necessary to derive $\boldsymbol{F}_{dipole}$ from $\phi$. [Refer to Eq. (4).] The force $\boldsymbol{F}_{dipole}$ applied to the polarized particle in the gradient field is determined by the following equation.[9]

$$\boldsymbol{F}_{dipole} = 4\pi\varepsilon_0 \frac{\varepsilon - 1}{\varepsilon + 2} R^3 \boldsymbol{E}_0 \nabla \boldsymbol{E}_0\ , \tag{4}$$

where $\varepsilon$ is a relative permittivity of the particle. The particle is assumed to be a dipole and force from other polarized particles is neglected, because particles usually do not distribute dense except for the initial condition. Figure 11 shows magnitudes of the Coulomb and polarization forces when the particle is on the conveyer and Fig. 12 is those at 250 µm apart from the conveyer. Although $\boldsymbol{F}_{dipole}$ is the same order of the Coulomb force at the conveyer surface, it is negligibly small when the particle locates at the position a little separated from the conveyer. That is, the Coulomb force is the most predominant driving force for air-borne particles. However, the polarization force plays an important role when particles are on the conveyer, especially at the start of the operation, because charge of particle is not large at the initial condition as shown in Fig. 4.

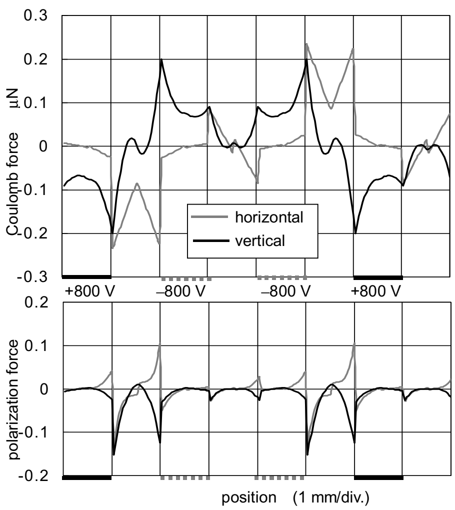


*Figure 11. Coulomb force and polarization force applied to particle at $z = 50$ µm. ($R = 50$ µm, $q = –0.06$ µC/g)*

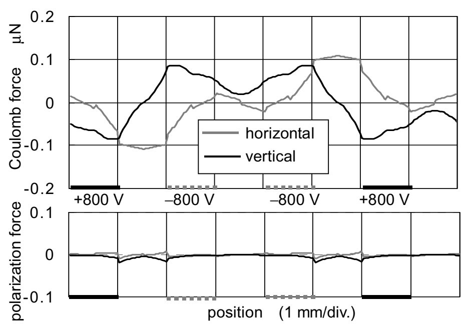


*Figure 12. Coulomb force and polarization force applied to particle at $z = 300$ µm. ($R = 50$ µm, $q = –0.06$ µC/g)*

Equation (2) is calculated with the Runge-Kutta method. During a time-step calculation, initial conditions are renewed when collisions between particle-particle and particle-conveyer take place. Linear and angular velocities after collision are calculated by a two-body impact equation that includes repulsive and frictional effects.

## Results and Discussion

### Transport Direction

Transport direction was categorized with three features, forward, backward, and non-transported.[1] At low frequency, particles were transported in the direction of the traveling wave propagation (forward direction) but at relatively high frequency particles transported backward increased. Motion of forward transported particles was almost synchronized with the traveling wave but that of backward was slow to the wave. Particles were not transported but only vibrated at higher frequency, herein a limitation for the transport existed. Figure 13 shows a comparison of measured and calculated macroscopic characteristics on the transport direction. Number of particles for the calculation was one hundred. The calculated agreed qualitative with the measured but some discrepancies existed. One was that the calculated transition frequency from the forward to backward transport was lower than the measured and another is that although small particles were apt to be transported forward even at high frequency in the experiment, the calculated was just opposite. Possible reasons of these disagreements are too small number of particles for calculations and neglect of adhesion force such as Van der Waals force.

### Transport Speed

Figure 14, 15, and 16 show a comparison of measured and calculated characteristics on the transport speed. Experimental results plotted in the figures were determined from several fastest particles reached to the end of the conveyer, on the other hand all of calculated particles were plotted in the figures.

Although the motion of particles is not simple and identical but a complex of many modes, the transport of particle ACM2107, for example, was roughly categorized with five modes with respect to the speed.

(1) Overtaking region: Some particle overtook the wave velocity at less than about 30 Hz.
(2) Synchronous region: Speed of major particles is same with the wave speed at about 30-50 Hz.
(3) Delay region: Many particles became to delay to the wave in accordance with the increase of the frequency at about 50-80 Hz, although major particles were transported forward.
(4) Backward transport region: Major particles were transported backward to the wave at 80-250 Hz.
(5) Vibration region: Particles were not transported but only vibrated at higher frequency, higher than 250 Hz.

### Modes of Dynamics

Microscopic differential dynamics of particles were observed and compared to calculations.

(1) Overtaking region: Figure 17 shows measured and calculated loci of particles and potential distribution on the surface of the conveyer in case of 10 Hz operation. The abscissa is a relative horizontal position to the wave, i.e. the position when an observer is on the wave that moves to the left side. Loci of several typical particles were measured with a high-speed microscope camera from a lateral direction of the conveyer. Although potential pockets existed, some particles in this region were not trapped in pockets but overtook the potential wave, because the speed of the wave was too slow compared to the particle speed.
(2) Synchronous region: Figure 18 shows measured and calculated loci of particles at 30 Hz and potential distribution on the conveyer surface. The abscissa is also the rela tive horizontal position to the wave. In this case, when the wave speed was moderate compared to the particle speed, particles were trapped in potential pockets and thus the speed of particles were synchronized with the wave speed.

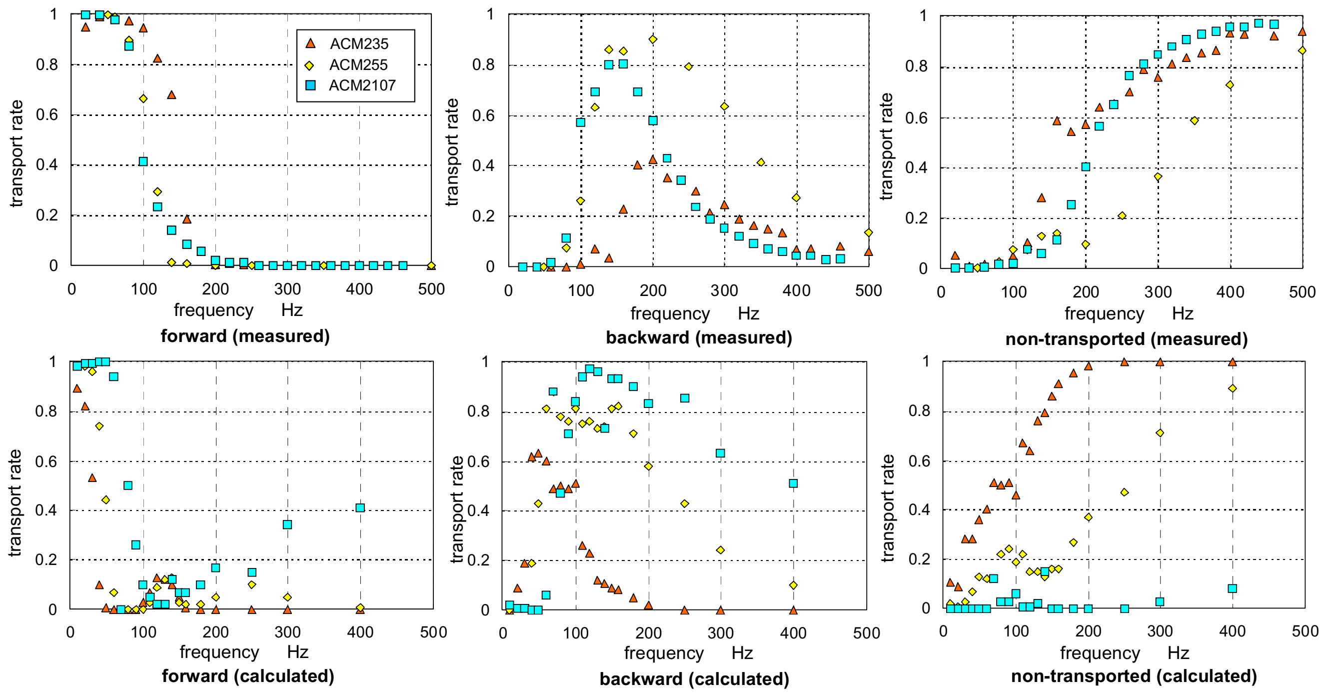


*Figure 13. Measured and calculated rates of forward, backward, and non-transported particles with respect to frequency of traveling wave.*

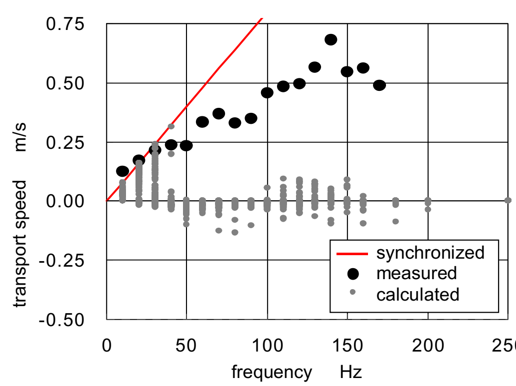


*Figure 14. Measured and calculated transport speed with respect to frequency of traveling wave. (ACM235)*

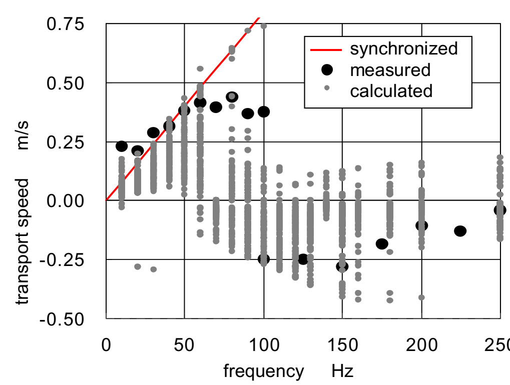


*Figure 16. Measured and calculated transport speed with respect to frequency of traveling wave. (ACM2107)*

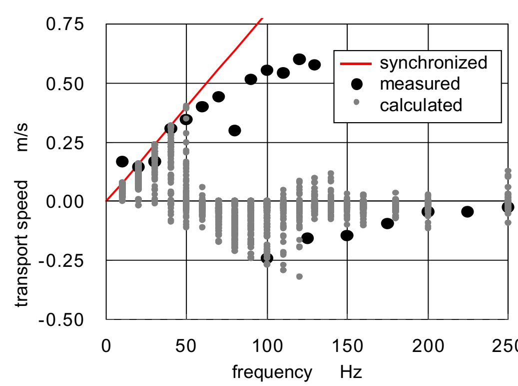


*Figure 15. Measured and calculated transport speed with respect to frequency of traveling wave. (ACM255)*

(3) Backward transport region: Figure 19 shows a calculated locus of particles at 140 Hz. We could not observe particle trajectories in this region, because our high-speed camera could not trace the high-speed particle motion. The potential distribution shown in this figure was not relative but ordinal, observed from the stationary coordinate, because it became a complex figure. Calculated locus clearly showed that the particles were transported backward at relatively low altitudes.

(4) Vibration region: Figure 20 shows calculated locus at 250 Hz and the ordinal potential distribution. Particles were not transported but only vibrated at a low altitude. This coincided with the experimental observation.

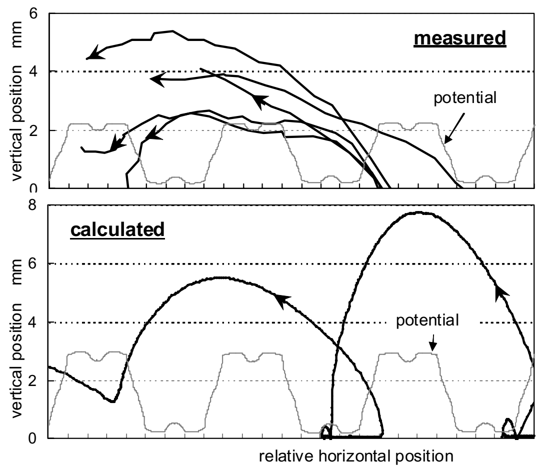


*Figure 17. Measured and calculated locus of particles at very low frequency. (10 Hz, ACM2107)*

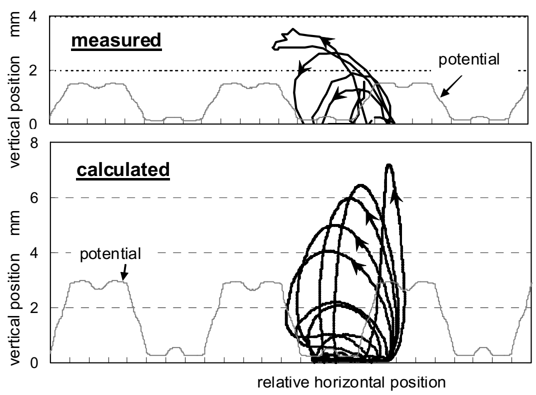


*Figure 18. Measured and calculated locus of particles at low frequency. (30 Hz, ACM2107)*

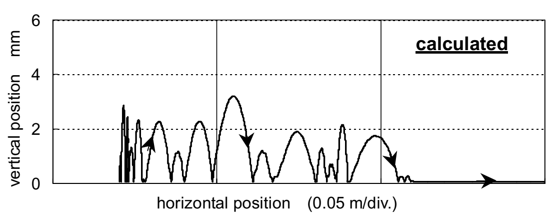


*Figure 19. Calculated locus of particles at medium frequency. (140 Hz, ACM2107)*

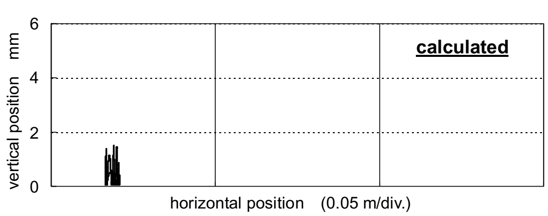


*Figure 20. Calculated locus of particles at high frequency. (250 Hz, ACM2107)*

## Concluding Remarks

Numerical and experimental investigations were carried out on transport of particles in an electrostatic traveling field. Although the motion of particles is not simple and identical but a complex of many modes, because it is affected by many parameters that include mechanical and electrical interactions between particle-particle and particle-conveyer, major characteristics are as follows:

(1) Particles were slightly charged when they were settled on the conveyer due to the static electrification. If the traveling field was applied, the Coulomb force and polarization force were applied to particles and then particles were driven and collided with each other and with the conveyer. This increased charge and polarization with time. The Coulomb force was most predominant to drive particles except when particles were on the conveyer.

(2) The direction of particle transport did not always coincide with that of the traveling wave but partially changed depending on the frequency of the traveling wave, the particle diameter, and the electric field.

(3) Although some particles overtook the traveling wave at the very low frequency, the motion of particles was almost synchronized with the wave at the low frequency.

(4) The transport of some particles delayed to the wave at medium frequency and almost all particles were transported backward at high frequency.

## Acknowledgement

This work is supported by The 21st Century COE Program of Japan Society for Promotion of Science.

## References

1. H. Kawamoto and N. Hasegawa, Traveling Wave Transport of Particles and Particle Size Classification, J. Imaging Sci. Technol. (to be published).
2. J. R. Melcher, E. P. Warren and R. H. Kotwal, Theory for Finite-Phase Traveling-Wave Boundary-Guided Transport of Triboelectrified Particles, IEEE Trans. Industry Appl, 25, 5 (1989) pp.949-955.
3. J. R. Melcher, E. P. Warren and R. H. Kotwal, Traveling-Wave Delivery of Single-Component Developer, IEEE Trans. Industry Appl, 25, 5 (1989) pp.956-961.
4. F. W. Schmidlin, A New Nonlevitated Mode of Traveling Wave Toner Transport, IEEE Trans. Industry Appl, 27, 3 (1991) pp.480-487.
5. S. Masuda, M. Washizu and M. Iwadare, Separation of Small Particles Suspended in Liquid by Nonuniform Traveling Field, IEEE Trans. Industry Appl, IA-23, 3 (1987) pp.474-480.
6. R. Kober, Transport geladener Partikel in elektrischen Wanderfeldern, Dissertation, Achen Univ. Technology (2003).
7. K. Taniguchi et al, A New Technique for Measuring the Distribution of Charge-to-Mass ration for Toner Particles with On-Line Use, J. Imaging Sci. Technol, 47, 3 (2003) pp.

On-Line Use, J. Imaging Sci. Technol, 47, 3 (2003) pp. 224-228.
8. L. B. Schein, Electrophotography and Development Physics (Revised Second Edition), Laplacian Press, CA (1996).
9. T. B. Jones, Electromechanics of Particles, Cambridge University Press, NY (1995).

## Biography

**Hiroyuki Kawamoto** holds a BS degree in Electrical Engineering from Hiroshima Univ.(1972) and a Dr. degree in Mechanical Engineering from Tokyo Institute of Technology (1983). From 1972 to 1991 he was a Senior Engineer at the Nuclear Division of Hitachi Ltd. In 1991 he moved to Fuji Xerox, and had been engaged in the research of electrophotography as a Research Fellow. In 1999 he left Fuji Xerox and he is now a professor of Waseda Univ. His awards include the Japan Society of Mechanical Engineers Young Scientist Award (1984), the 7th International Microelectronics Conf. Best Paper Award (1992), the Japan Institute of Invention and Innovation Patent Award (1993), and the 10th International Symposium on Applied Electromagnetics and Mechanics Award for Outstanding Presentation Paper (2001). He was selected a Fellow of the IS&T in 1999 and also a Fellow of the Japan Society of Mechanical Engineers in 2004.